doi:10.1016/j.jmb.2005.12.015 J. Mol. Biol. (2006) 356, 1207–1221

JMB

Available online at www.sciencedirect.com

SCIENCE DIRECT®

ELSEVIER

Effects of Solubilization on the Structure and Function of the Sensory Rhodopsin II/Transducer Complex

Johann P. Klare[1], Enrica Bordignon[2], Meike Doebber[2], Jörg Fitter[3] Jana Kriegsmann[3], Igor Chizhov[4], Heinz-Jürgen Steinhoff[2]* and Martin Engelhard[1]*

[1]*Max-Planck-Institut für Molekulare Physiologie Otto-Hahn-Str. 11, 44227 Dortmund, Germany*

[2]*Fachbereich Physik, Universität Osnabrück Barbarastrasse 7, 49069 Osnabrück, Germany*

[3]*Forschungszentrum Jülich IBI-2: Strukturelle Biologie 52425 Jülich, Germany*

[4]*Medizinische Hochschule Hannover, Inst. für Biophysikalische Chemie Carl-Neuberg-Str. 1 30623 Hannover, Germany*

**Corresponding authors*

Lipid–protein interactions are known to play a crucial role in structure and physiological activity of integral membrane proteins. However, current technology for membrane protein purification necessitates extraction from the membrane into detergent micelles. Also, due to experimental protocols, most of the data available for membrane proteins is obtained using detergent-solubilized samples. Stable solubilization of membrane proteins is therefore an important issue in biotechnology as well as in biochemistry and structural biology. An understanding of solubilization effects on structural and functional properties of specific proteins is of utmost relevance for the evaluation and interpretation of experimental results. In this study, a comparison of structural and kinetic data obtained for the archaebacterial photoreceptor/transducer complex from *Natronomonas pharaonis* (NpSRII/NpHtrII) in detergent-solubilized and lipid-reconstituted states is presented. Laser flash photolysis, fluorescence spectroscopy, and electron paramagnetic resonance spectroscopy data reveal considerable influence of solubilization on the photocycle kinetics of the receptor protein and on the structure of the transducer protein. Especially the protein-membrane proximal region and the protein–protein interfacial domains are sensitive towards non-native conditions. These data demonstrate that relevance of biochemical and structural information obtained from solubilized membrane proteins or membrane protein complexes has to be evaluated carefully.

Keywords: phoborhodopsin; phototaxis; membrane proteins; site-directed spin labeling EPR; detergents

Introduction

Integral membrane proteins, comprising 20–30% of all proteins present in cells,[1] exhibit a fundamental role in cell–cell communication, information exchange with the environment, or energy transduction. Their properties and location within the cell membrane have made them a valuable target for therapeutic drugs.[2] Despite their considerable importance, the elucidation of their functional and structural properties was, and still is, hampered by the fact that purification procedures dissolve the proteins out of the membrane into a milieu different from that of the native lipid bilayer. This crucial step is generally done by solubilization with detergent, which, in quite a few cases, destroys the stability of the target membrane protein. This restriction in studying membrane proteins is one of the reasons that only few of them have been crystallized. Only about 95 different membrane proteins have been deposited in the Protein Data Bank, overwhelmingly from bacterial sources. A further constraint for the analysis of membrane proteins is that some

J.P.K. & E.B. contributed equally to this work.

Abbreviations used: NpSRII, *Natronomonas pharaonis* sensory rhodopsin II; $NpHtrII_{157}$, *Natronomonas pharaonis* halobacterial transducer of rhodopsins II truncated at residue 157; HAMP domain, conserved signal transduction domain in histidine kinases, adenylyl cyclases, methyl-accepting chemotaxis proteins and phosphatases; PML, purple membrane lipids; DDM, β-dodecyl-D-maltoside; MTSSL, methanethiosulfonate spin label (the spin label side-chain is also abbreviated as R1); MW, microwave; SDSL, site-directed spin labeling; EPR, electron paramagnetic resonance.

E-mail addresses of the corresponding authors: hsteinho@uos.de; martin.engelhard@mpi-dortmund.mpg.de

biophysical or biochemical techniques afford a solubilized sample. For example, absorption spectroscopy, circular dichroism, and high-resolution NMR are applicable only for dissolved probes.

The difference between a detergent and a cellular lipid environment is mainly due to two particularities of the latter system. Membranes, in contrast to detergents, have three distinct zones. A non-polar hydrophobic region separates two hydrophilic and charged boundaries facing the aqueous solution. A second feature that influences protein function and stability is probably the membrane potential, which is generally around −100 mV. Clearly, voltage sensors like the voltage-dependent potassium channel (KvAP) belong to those membrane proteins affected. Also, a voltage dependence was observed for the proton pump activity of bacteriorhodopsin.[3] These examples show the necessity to study membrane proteins in conditions as similar to the native environment as possible.

Since quite a few data have been obtained from studying membrane proteins under non-native conditions, it is important to address the question of how reliable these results are and if they are reflecting the properties of the protein *in vivo*. This is especially important because a wealth of biochemical and biophysical information is available for solubilized membrane proteins, data that has to be shown to be relevant for the proteins in their native environment. Although these difficulties of data interpretation have been addressed in recent years,[4–12] very few detailed comparative studies have been published.[7,8]

The membrane protein pair under investigation in the present study, sensory rhodopsin, an archaebacterial photoreceptor from *Natronomonas pharaonis* (NpSRII), and its cognate transducer (NpHtrII), has been analyzed both in the lipid-reconstituted state and as a solubilized probe. NpSRII, a seven transmembrane helix (A–G) protein, mediates the photophobic response of *N. pharaonis* to green-blue light under aerobic conditions and forms a complex with NpHtrII in a 2:2 stoichiometry in membranes (see Figure 1).[13–17] Activation by light leads to isomerization of the retinal chromophore, which is followed by a sequence of intermediates, finally leading back to the original ground state. In analogy to the bacteriorhodopsin photocycle, these intermediates were named K, L, M, N, and O. A model of the photocycle included a spectrally silent transition between two M states ($M_1 \rightarrow M_2$), which has been proposed to generate the active signaling state.[18] This transition is accompanied by an outward movement of helix F,[19,20] which is suggested to trigger a conformational change of the associated transducer molecule resulting in a rotational or screw-like motion of its second transmembrane helix (TM2). This signal then propagates in an unknown mechanism to the cytoplasmic apex of the transducer molecule, where it modulates, in analogy to the chemotactic system of enteric bacteria like *Escherichia coli*, the autophosphorylation activity of the bound His-kinase CheA,[21] and finally affects the swimming behavior of the cell by means of a two-component signal transduction machinery.

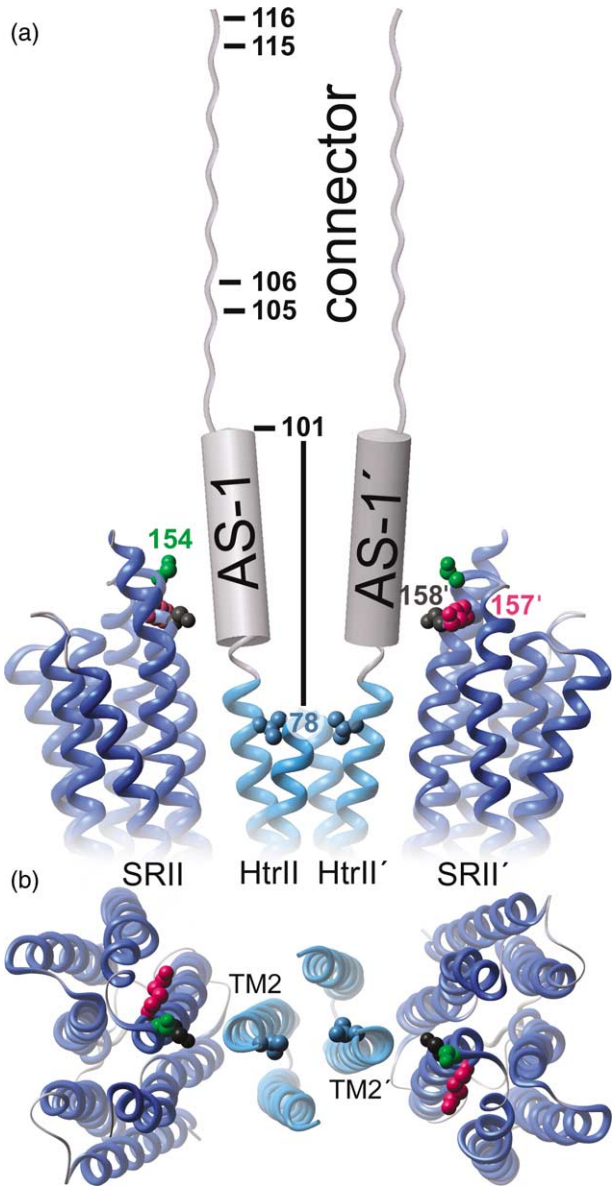

Figure 1. (a) A cartoon representation of the 2:2 NpSRII/NpHtrII complex. The colored ribbon represents the X-ray structure (PDB 1H2S) of the transmembrane domain of the complex (NpSRII, blue; NpHtrII, cyan); a representation of the AS-1 and connector regions of the transducer up to position 116 perpendicularly to the membrane plane into the cytoplasmic phase is depicted in gray. For clarity, the predicted α-helical sequence AS-1 and the extended connector region are stretched according to the number of residues. Positions in the receptor and in the transducer subjected to the SDSL EPR study are indicated. Side-chains on the NpSRII subjected to study are shown (S154, K157, S158) as ball representation; the residue V78 in the transducer is also depicted. (b) Ribbon representation of the X-ray structure of the transmembrane domain of the complex, top view.

The functional and structural properties of the NpSRII/NpHtrII complex have been studied mostly in the detergent-solubilized state, generally by using *n*-dodecyl-β-D-maltoside (DDM). All binding constants determined for the interaction between receptor and transducer (either by means of transducer-caused changes of the NpSRII M-decay or calorimetric studies),[22–24] as well as for mutants of one or both of the proteins,[25–27] are obtained just for solubilized samples. Also, recent studies addressing the structure of the transducer linker region and its interaction with the receptor were carried out with solubilized proteins.[23,28]

The complex formed by NpSRII and NpHtrII has been crystallized in a 2:2 ratio in the membrane,[29] and it has been shown by site-directed spin labeling (SDSL) electron paramagnetic resonance (EPR) to be at least dimeric also at room temperature and at low temperature when reconstituted in purple membrane lipids (PML) (see Figure 2).[30] The dimerization allows the interaction between the long cytoplasmic regions of two adjacent transducers to take place *in vivo*, leading to the formation of a four helix bundle structure analogous to the chemotaxis receptors in *E. coli*.

It has been shown that detergents interfere with the stoichiometry and stability of the receptor/transducer complex. In contrast to reconstituted samples, NpSRII/NpHtrII exhibits only a 1:1 stoichiometry in DDM.[22,30] Considering the thermal stability of NpSRII and the NpSRII/NpHtrII complex, Sudo and co-workers reported that lipids as well as the transducer have a stabilization effect on the receptor.[31] These observations provide an opportunity to study the influence of detergents on the functional and structural properties of the NpSRII/NpHtrII complex in more detail. Data from laser flash photolysis, fluorescence spectroscopy, and EPR spectroscopy reveal that protein–protein contacts and the protein–buffer interface are altered by treatment with detergents.

Results

Photocycle kinetics

Flash-induced absorption changes of NpSRII and its complex with $NpHtrII_{157}$ in solubilized and reconstituted forms recorded at representative wavelengths are shown in Figure 3. The trace at 500 nm represents depletion and recovery of the ground state, the tract at 400 nm displays the rise and decay of the M-intermediate, whereas the O-intermediate was monitored at 550 nm. The data presented in Figure 3 do not show significant differences in the M-formation kinetics upon solubilization or transducer binding. On the other hand, Sasaki and Spudich described an influence on the L–M transition in the HsSRII photocycle upon transducer binding.[32] The most probable cause, other than using different proteins (HsSRII *versus* NpSRII in the present study) and different concentrations of salt (high *versus* low concentration of NaCl, respectively), might be the different temperature dependence of the kinetics describing the L–M transition of HsSRII with and without its transducer. At a temperature range of 20–25 °C, these rates become almost identical.[31] Since the present photocycle experiments were carried out at 25 °C and assuming a similar behavior of the *N. pharaonis* proteins, the difference from the work of Sasaki and Spudich can be explained.

In contrast to the first part of the photocycle, the M-decay is much more sensitive towards external conditions. In the solubilized forms, the decay of the M-intermediate is slowed by a factor of 2–3 as compared to the PML-reconstituted samples. This

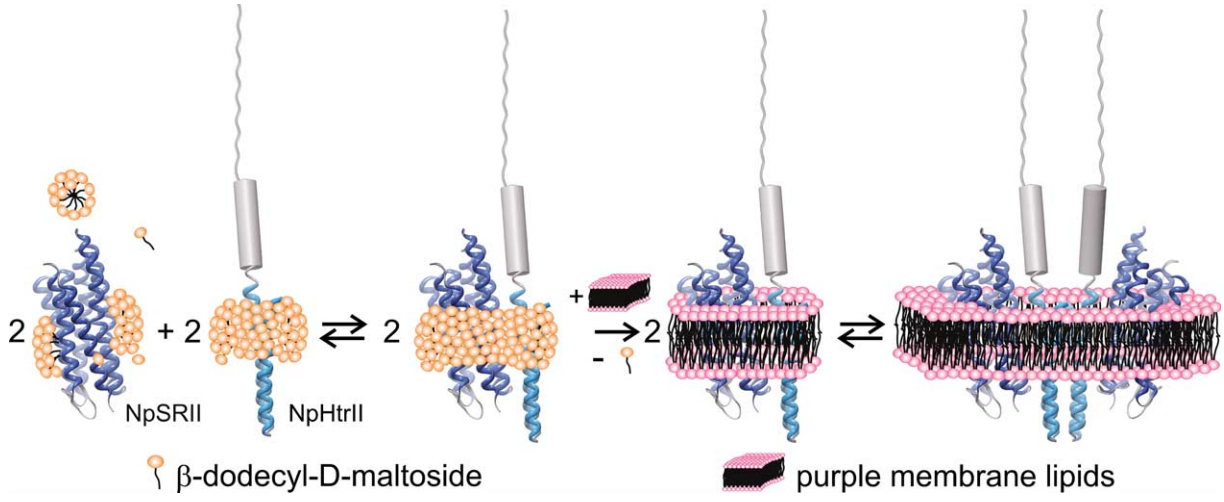

Figure 2. A cartoon representation of the solubilized and reconstituted samples in the experimental procedure adopted for the reconstitution of NpSRII (blue ribbon diagram from the PDB file 1H2S) and $NpHtrII_{157}$ (a cartoon representation of the transducer up to position 116 from Figure 1). Both proteins are first isolated independently in DDM micelles, then mixed together to form a 1:1 complex. For reconstitution into purple membrane lipids (PML), the mixture is shaken in a buffer containing a 40-fold excess of lipids as well as detergent-absorbing Biobeads.

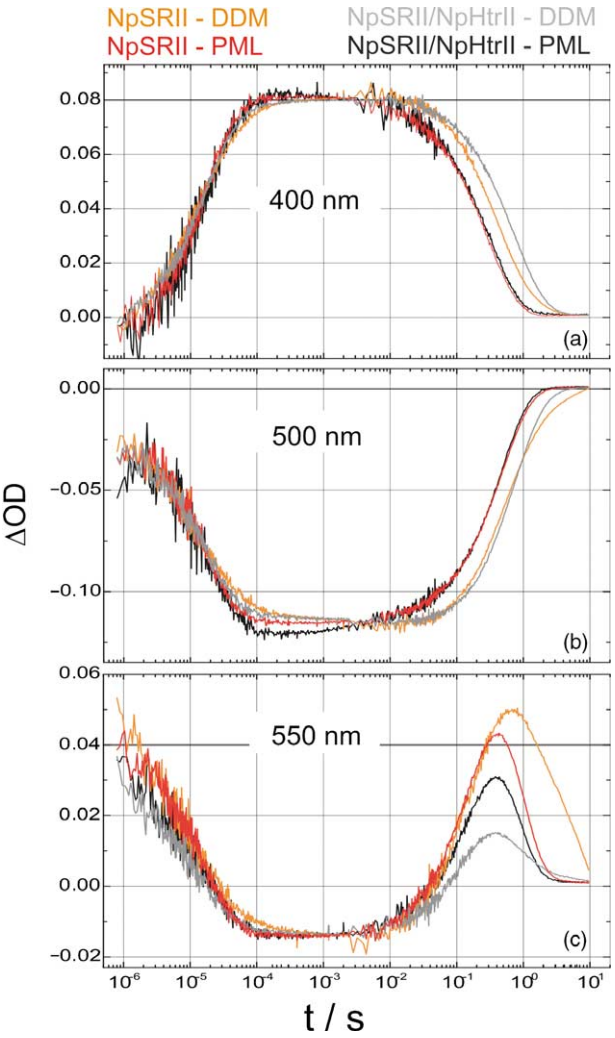

Figure 3. Traces of transient absorption changes after photoexcitation of NpSRII in DDM-solubilized (orange traces) and in PML-reconstituted (red traces) forms, NpSRII/NpHtrII$_{157}$ in DDM-solubilized (gray traces) and in PML-reconstituted (black traces) forms. Traces are recorded at 25 °C at wavelengths characteristic of the sensory rhodopsin photocycle: 400 nm (M state), 500 nm (ground state) and 550 nm (O state).

observation is in line with previous results, which were used to analyze the dissociation constant of the receptor–transducer complex.[33] The transducer binding affects the M decay in the solubilized samples, while no effect is observable in the reconstituted moieties.

The rise and the decay of the O-intermediate show some subtle changes, depending on the environment of the receptor. Solubilization of the receptor alone (Figure 3(c)) leads to a clear change of the decay kinetics of this intermediate compared to the membrane-bound protein, resulting in a prolonged photocycle turnover of this sample (Figure 3(b)). However, for the complex, the transient amount of the O-intermediate changes but not the lifetime of this state. The clear difference in the amplitude observed at 550 nm indicates a strong influence of the solubilization on the equilibrium between M and O. The observation that binding of the transducer accelerates the O decay in the solubilized complex is in line with previous work on HsSRII,[32] but, interestingly, this feature cannot be observed for the reconstituted samples, where transducer binding does not further influence the photocycle. Whether this effect can be ascribed to the specific species differences or to the truncation performed on the transducer will be further investigated.

Clustering of receptor–transducer complexes in lipids

The red-absorbing fluorophore Atto655 was utilized to monitor the local environment of position 157 in the cytoplasmic edge of helix F (see Figure 1 for its location). A comparison of fluorescence emission

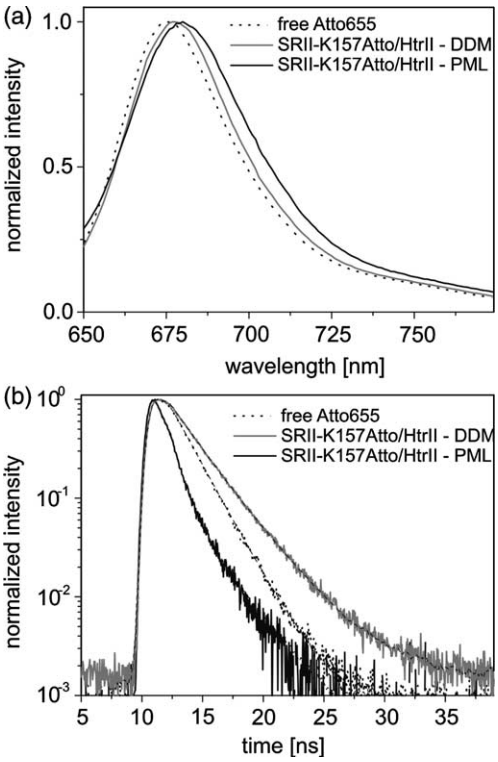

Figure 4. Fluorescence emission spectra and fluorescence lifetime decays for the free Atto655 dye and for the dye attached to position 157 in NpSRII in complex with NpHtrII. (a) Fluorescence emission spectra of free dye in detergent buffer (black dotted line), dye attached to the receptor in detergent-solubilized NpSRII/NpHtrII$_{157}$ complexes (gray line), and in PML-reconstituted complexes (black line). (b) The lifetime decay of Atto655 in detergent-free buffer (black dotted line) exhibits a mono-exponential decay ($\tau = 1.9$ ns); the dye attached to the receptor shows a distinct deviation from mono-exponential decay in both states. With respect to the complex in detergent (with longer decay as compared to the free dye, gray line) the complex reconstituted in PML shows a drastically shortened lifetime decay (black line). The broken black lines represent fits of a mono-exponential decay of the free dye and multi-exponential decays (two and three components) of the bound dye.

spectra and lifetimes (Figure 4) of the free fluorophore in solution or bound to the PML-reconstituted and DDM-solubilized NpSRII/NpHtrII complex reveals information on the local environment of position 157. With respect to the free dye, the emission spectrum of the dye bound to the DDM-solubilized complex shows a slight red shift of the order of 1–2 nm. An even more pronounced red shift is observed for the complex reconstituted in PML with $\Delta\lambda_{max}=4$ nm (Figure 4(a)). A distinct difference between the solubilized and reconstituted complexes is visible also in the dye lifetimes (Figure 4(b)). The free Atto655 in buffer solution is characterized by a mono-exponential decay ($\tau=1.9$ ns), which is rather insensitive to the presence of detergent in the buffer (data not shown). The fluorophore bound to the DDM-solubilized complexes exhibits a significantly increased lifetime, which is typically observed in hydrophobic environments.[34]

In contrast, the complexes reconstituted in lipids are dominated by a much shorter lifetime component and show an additional longer decay component similar to that observed in detergent samples. The two components indicate two different populations either on the level of the protein complex or on that of the fluorophore. In either case, the slow component can be explained by a hydrophobic environment like that observed in detergents. The fast decay observed probably arises from quenching by a nearby chromophore. It is well known that contact formation between tryptophan and Atto655 gives rise to significant quenching of the Atto-fluorophore (electron transfer-based fluorescence quenching) visible as shortened lifetimes and red-shifted emission spectra.[35] Although Atto655 exhibits a spatial extension of about 14 Å (including the maleimide linker group), no tryptophan residue is reachable within the receptor–transducer complex suitable for such an energy transfer process. However, if one assumes an inter-complex contact occurring in membranes, the fluorophore can come into contact with W24, which is located in helix A on the opposite side of the receptor. This interpretation is supported by the observation that NpSRII/NpHtrII$_{157}$ reconstituted into DMPC vesicles at a much lower protein to lipid ratio (1/10) shows a similar, but weaker, quenching of the dye (data not shown). Similar results were obtained from pulse-EPR measurements (DEER), which indicate the presence of higher-order structures in membranes (unpublished data). Apparently higher-order clusters, which are suggested to be relevant for signal transduction, are formed only in the presence of membranes.[36,37]

Effects of solubilization on the complex stoichiometry

Oligomerization of membrane proteins *in vivo* has been observed for quite a few examples, e.g. bacteriorhodopsin, which forms a two-dimensional crystal consisting of trimers in its native purple membrane,[38] or chemotactic receptors like Tsr or Tar from *E. coli*, whose cluster formation is thought to be associated with the sensitivity of the signaling cascade.[39] These higher-order structures might be severely affected by the treatment with detergents, as it has been shown for the NpSRII/NpHtrII$_{157}$ complex.[24,30]

In order to further investigate the effect of the lipid bilayer on the aggregation state of the NpSRII/NpHtrII$_{157}$ complex, we first analyzed if the transducers alone form dimers in lipid membranes. In a previous EPR study on the NpSRII/NpHtrII$_{157}$ complex it was shown that a spin label at position 78 (NpHtrII$_{157}$-V78R1) is well-suited to monitor a possible dimerization.[30] In a dimer, the spin label would be located in the transmembrane region at the interface between helices TM2 and TM2′ (see Figure 1) at a distance of about 1.2 nm.[30]

In the present study, we compared the room-temperature and low-temperature (160 K) EPR spectra of NpHtrII$_{157}$-V78R1 in the absence of NpSRII, being either solubilized or reconstituted in membranes. These measurements allow us to analyze motional freedom of the spin label at this site as well as evaluating spin–spin interactions, which provide information about inter-site distances (Figure 5).

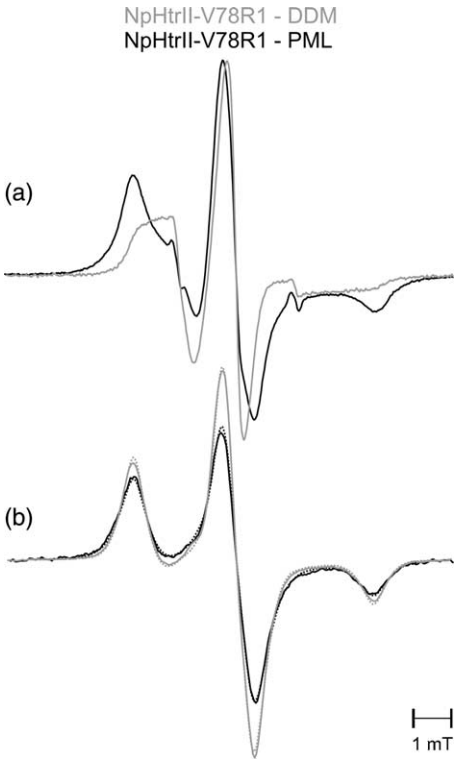

Figure 5. (a) Room-temperature and (b) low-temperature EPR spectra of NpHtrII$_{157}$-V78R1 in DDM-solubilized (gray line) and PML-reconstituted (black line) states in the absence of NpSRII. The room-temperature spectra are normalized to one at the maximum of intensity, the low-temperature spectra are normalized by spin number. The fitting of the simulated powder spectra is superimposed on the low-temperature spectra (dotted lines; for the parameters used, see Materials and Methods). The distance obtained in the NpHtrII$_{157}$-V78R1 PML reconstituted sample is 1.3($\pm$0.2) nm; the fraction of the singly labeled species amounts to 57%.

The room-temperature spectra of $NpHtrII_{157}$-V78R1 in the absence of the receptor in the detergent-solubilized and in the reconstituted forms (Figure 5(a)) are almost identical with those obtained in the analogous preparations of the complex (Figure 7, right panel). The 2:2 complex shows a spectrum indicating a high degree of immobilization of the spin label. The restriction in mobility for this residue, pointing to the opposite direction with respect to the receptor, is mainly due to the close vicinity to TM2′ in the 2:2 complex (see Figure 1). The higher degree of mobility observed for position 78 in the solubilized complex (Figure 7) indicates that this interaction is lost after solubilization, as expected. The similarities observed in the spectra in the presence and in the absence of receptor indicate that the intra- and intermolecular interactions for position 78 are not affected by the presence of NpSRII.

Moreover, we observed dipolar interaction at low temperature for the transducer alone reconstituted in membrane, which is not detectable in the analogous solubilized form (Figure 5(b)). The fitting of the simulated spectrum to the experimental one gives a distance slightly larger (1.3($\pm$0.2) nm) than that obtained in the complex,[30] nevertheless indicating that the transducers alone do interact and dimerize when reconstituted in membrane, even in the absence of the receptor. The dimer formed is less tight than that existing in the presence of the receptor in the complex and, similarly, it is disrupted after solubilization.

Effects of solubilization on the structural properties of NpSRII and $NpHtrII_{157}$

In order to analyze in more detail how solubilization affects the cytoplasm-exposed NpSRII domain, three residues in the cytoplasmic edge of helix F (S154, K157, and S158) have been chosen (Figure 1). The residues were mutated to cysteine, subsequently labeled with MTS SL and analyzed by SDSL EPR spectroscopy. Experiments were performed with solubilized and PML-reconstituted NpSRII either alone or in complex with $NpHtrII_{157}$. It should be noted that the introduction of a spin label at the majority of positions investigated so far seems not to interfere dramatically with the overall fold, the thermal stability or the function of a given protein.[40,41] Also, in the present study an effect of spin label modification on the photocycle kinetics was not observed at selected positions (data not shown).

The shape of the EPR spectra measured at room temperature reveals the degree of the nitroxide mobility, which depends on the protein structure in the vicinity of the spin label-binding site.[40,42,43] The term mobility is used in a general sense, and it accounts for the rate, amplitude and anisotropy of the spin label reorientational motion on the nanosecond timescale. In the case of residues buried in the interior of proteins, the motion of the spin label is restricted, due to strong interactions with neighboring side-chains or backbone atoms; thus, the EPR spectral linewidths and apparent hyperfine splitting are large. In the case of helix surface sites, where the spin label is exposed either to the water or to the lipid phase, the EPR spectra are characterized by smaller linewidths, indicative for a relatively high mobility of the spin label side-chain.[44] In loop regions, random coil structures and helix termini, the EPR linewidths and apparent hyperfine splittings are small due to the absence of tertiary interactions with neighboring residues. Additionally, the intrinsic degree of flexibility of these secondary structures may contribute to the observed dynamics of the spin label.[45,46] When considering small proteins in solution, their overall tumbling (occurring on the nanosecond timescale) can also affect the EPR spectral shape; to examine in these cases the motion of the nitroxide relative to the protein, the contribution of the protein rotation to the EPR line shape can be reduced by adding 30% (w/w) sucrose.[47]

Figure 6 shows the comparison between the continuous wave (cw) X-band spectra obtained for each mutant at room temperature in the four different states. The spin labels at positions 157 and 158 are characterized by strong interactions with nearby groups. The spin label attached at position 154 near the EF loop region shows a higher degree of mobility, thus indicating a weaker interaction with neighboring residues.

Interestingly, all spectra show the presence of at least two spectral components, which has already been observed for spin labels attached at interfacial regions in other proteins.[48] Although one can assume that one of these components represents an unfolded or misfolded species present in the sample, ITC measurements on solubilized samples had shown a 1:1 stoichiometry for the transducer binding to the receptor without any indication for the presence of two different binding modes.[24] One can deduce from this experiment that even if two species are present they do not have different modes of binding to the receptor, indicating a similar protein–protein binding interface within the complex. Moreover, an influence of temperature and salt concentration on the distribution of the two spectral components has been detected. These two states might represent different signaling states of the transducer protein.[46]

Comparing the spectra from NpSRII alone, it is evident that solubilization induces only a slight increase in the mean mobility of the spin label, which might arise from a slight change in the environment surrounding the label and from the decreased rotational correlation time of the detergent-solubilized sensory rhodopsin moiety. For the micelle-embedded NpSRII, a rough estimate of the rotational correlation time based on the Stokes-Einstein-Debye relation gives 16 ns (for the calculation we used a specific volume of 0.765 $cm^3\,g^{-1}$ estimated for the rhodopsin/detergent complex and a content of 0.97 g of detergent /g of protein[49] leading to 50 DDM molecules per NpSRII, in accord

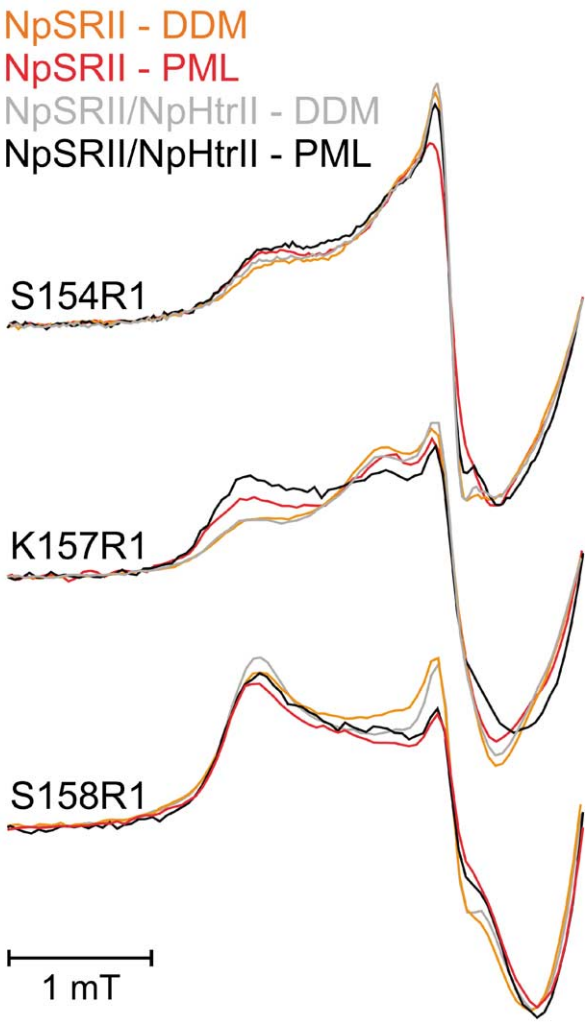

Figure 6. Room-temperature EPR spectra of the NpSRII mutants S154R1, K157R1, and S158R1 in NpSRII DDM-solubilized (orange traces) and PML-reconstituted (red traces), NpSRII/NpHtrII$_{157}$ DDM-solubilized (gray traces) and PML-reconstituted (black traces). For clarity, only the low-field region of the spectra is compared. The spectra are normalized to one at the maximum of intensity of the central peak (not shown).

with values found for solubilized BR[50]). When comparing the spectra of the NpSRII/NpHtrII$_{157}$ in the solubilized and in the PML-reconstituted forms, it is evident that the interactions, which determine the spectral shape, are slightly changed for position 157 only. This suggests that the changes induced by solubilization in the cytoplasm-exposed domain of NpSRII are of minor relevance. The minimal increase in mobility observed for positions 154 and 158 may arise from the estimated 25 ns rotational correlation time of the 1:1 complex in detergent.

The presence of the transducer in both the solubilized and reconstituted complex seems not to perturb the overall shape of the spectra, except for position 157, which shows a slight decrease in the mean mobility in the reconstituted sample. This indicates that the interactions restricting the motion in the positions under investigation are mainly intramolecular, and the interactions of this part of the receptor with the cognate transducer are negligible.

To further investigate the influence of the solubilization on the overall architecture of the NpSRII/NpHtrII$_{157}$ complex, we focused on the cytoplasm-exposed transducer region, thought to be crucial for the signal transduction. We chose 24 residues in the membrane-adjacent part of the transducer, from position 78 to position 101, and four residues in the following region (L105, D106, D115 and E116) to apply SDSL EPR. This selection was made on the grounds that X-ray data are available only up to residue 82 (see Figure 1), leaving the remainder of the cytoplasmic fragment completely undetermined.

The spectra of the solubilized complexes show distinct differences in comparison to those of the reconstituted complexes (see Figure 7). Generally, the spectral changes induced by solubilization are distinctive for each residue, depending on their specific location. In Figure 8(a), the mobility parameter is plotted against the residue number for both the solubilized (gray) and reconstituted (black) complex.

In general, the mobility parameter is higher for the solubilized complex than for the membrane-embedded sample. The significance of these changes arises if the relative differences (based on the absolute value of ΔH_0^{-1} of the reconstituted samples) are taken. The mobility value for position V78 is increased by 120% and all the other observed changes are in the range of 10–50%, most of them being about 40–50%. This indicates clearly that significant structural changes in the side-chains are induced by solubilization even in a region that is thought to be located at a reasonable distance from the membrane/micelle.

As described above, the close interaction existing in the reconstituted 2:2 complex between the transmembrane region of TM2 and TM2′,[29,30] which restricts the rotational motion of the nitroxide attached at the interfacial sites, is clearly lost in the solubilized 1:1 complex, where helix TM2′ is replaced by detergent molecules. The spectral changes expected for the residues comprising the end of the membrane-embedded part of TM2 (V78-L82) should then reflect the absence of TM2′. Indeed, a higher mobilization is observed for residue V78, located at the dimerization interface, while no effect is visible for residue T81 pointing towards the receptor.

However, also the transducer residues L82–A94, clearly protruding from the receptor–transducer interface and the membrane–micelle region, are affected, showing an increase in the mobility parameter ranging from 0.5 mT^{-1} for residues G83-A87 up to 1.5 mT^{-1} for the following region up to residue A94. The general increase in mobility observed in this region might be explained by the

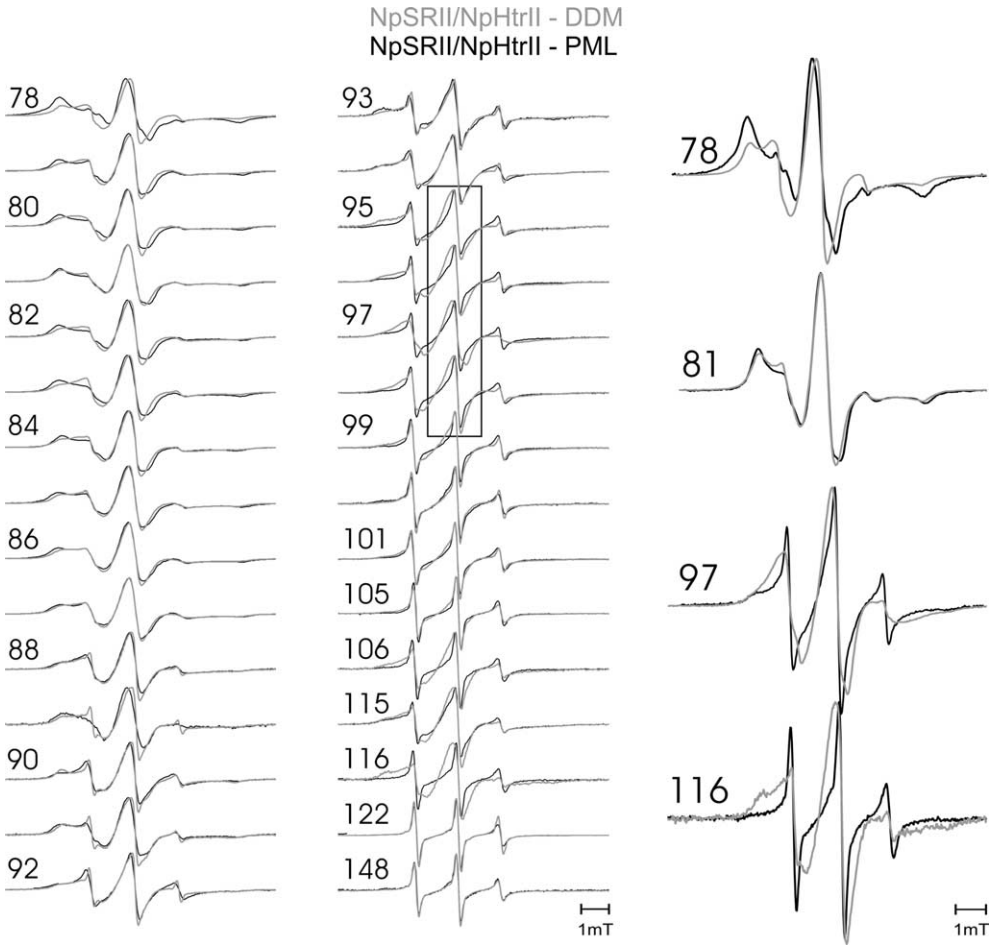

Figure 7. Comparison between the room-temperature EPR spectra of the $NpHtrII_{157}$ mutants in complex with NpSRII reconstituted in PML (black line) and solubilized (gray line). The spectra are scaled to equal (positive) amplitude of the central resonance peak. The spin-labeled mutants are designated by the residue number at which the nitroxide is introduced. The analyzed positions are located in the TM2 helix of the transducer (78–82), in the AS-1 sequence (83–101) and in the connector region (105, 106, 115, and 116). "The box highlights the first protein segment for which a decrease in the mobility is observed upon solubilization (positions 95–98). Selected spectra (78, 81, 97, and 116) representative of the different spectral changes induced by solubilization are magnified on the right.

loss of tertiary contacts with the cognate transducer. In fact, interactions between the two transducers have been detected in the 91–94 region in the reconstituted complexes.[46] However, additional conformational changes leading to an increase in the motional freedom of the spin labels cannot be excluded.

In contrast to that, for the region A95–S98, solubilization causes a strong decrease of the side-chain mobility, with its minimum observed position 97. A slight increase in the mean mobility is again observed for residues R99–G101, while for a consistent decrease in the main mobility after solubilization is detected for the analyzed positions in the 105–116 region. The strong decrease in mobility is indicative for the appearance of tertiary interactions with nearby residues restricting the spin label motion. In the absence of the second transducer, such interactions might arise either from the transducer region following the AS-1 sequence, which could bend towards the membrane, or from residues located in the receptor. Interestingly, the dynamics observed clearly differ from those obtained for the same positions in the reconstituted complex, suggesting relevant conformational changes occurring in the transducer upon solubilization.

To better describe the changes induced in the transducer by solubilization, the motional analysis performed was supplemented by measuring the collision frequency of diffusing paramagnetic probe molecules, quantified by the method of continuous wave power saturation. CrOx accessibility measurements performed on the membrane-adjacent transducer region A95–G101 clearly show that this part of the transducer is less accessible to the water phase in the solubilized complex, while oxygen accessibility shows no relevant changes with respect to the values in the reconstituted form (Figure 8(b)). This additional information confirms the structural changes suggested to take place in the transducer after solubilization, indicating the appearance of tertiary interactions between the transducer and neighboring residues, which hinder the CrOx accessibility towards the spin labels.

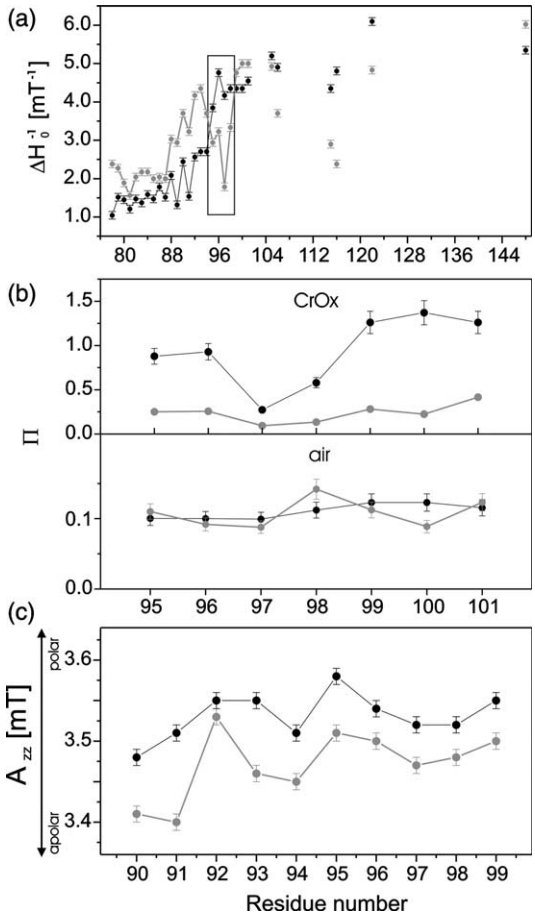

Figure 8. Comparison of mobility, accessibility and polarity data from selected positions of the transducer in the NpSRII/NpHtrII$_{157}$ complex in the reconstituted (black circles) and solubilized (gray circles) forms. (a) Plot of the mobility parameter obtained from the spectra in Figure 7. The estimated error is ± 0.01 mT^{-1}. The box highlights the first protein segment for which a decrease in the mobility is observed upon solubilization (positions 95–98, see Figure 7). (b) Plot of the accessibility values Π obtained for CrOx and air (21% oxygen) for positions 95–101. The estimated error is 10%. (c) Plot of the A_{zz} parameter obtained for positions 90–99 from the analysis of the low-temperature spectra (two selected low-temperature spectra for positions 93 and 95 are presented in Figure 9(a)). The estimated error is ± 0.1 mT.

Additionally, from the low-temperature EPR spectra detected on the singly spin-labeled transducer in the region L90–R99 in the solubilized and reconstituted complex, we measured the A_{zz} component of the hyperfine tensor, which is sensible to polarity changes in the environment of the spin label.[51,52] The lower A_{zz} parameter found for all residues in the solubilized form indicates a decrease in polarity of the environment of the transducer side-chain, according to its lower accessibility to the aqueous phase (Figure 8(c)).

To specify the entity of the structural changes induced by the solubilization in the membrane-adjacent region of the transducer, doubly labeled variants of the complex with R1 side-chains at positions 154 in the EF loop of the receptor and 93 or 95 in the transducer have been analyzed. The low-temperature spectra of the reconstituted complexes show the absence of close interaction (<2 nm) between the receptor and the transducer in the two double mutants (Figure 9(b)) when compared to the spectra of the singly labeled transducers in analogous preparations (Figure 9(a)). In the solubilized complexes, no relevant change is seen for the double mutant NpSRII-S154R1/NpHtrII$_{157}$-L93R1 with respect to the reconstituted complexes (Figure 9(b)); the slightly higher intensity of the central peak reveals the disruption of the 2:2 complex, hence the disappearance of the interaction present between positions 93 and 93′ in the transducers (visible for position 93 in Figure 9(a)). On the contrary, the spectrum from the double mutant NpSRII-S154R1/NpHtrII$_{157}$-A95R1 shows the appearance of dipolar broadening in the solubilized sample (fitting reveals distance values of 1.5($\pm$0.2) nm), despite the disruption of the 2:2 complex. The entity of the dipolar broadening in the double mutant spectrum, hence the interaction between the receptor and the transducer in the 1:1 complex, appears when comparing the height of the central peak with that of the spectrum of the analogous preparation of the singly labeled complex at position 95 in the transducer. The clear indication of an interaction between positions 154 in the receptor and 95 in the transducer in the solubilized complex further defines the structural changes induced by solubilization in the transducer region. The membrane-adjacent part of the transducer is in closer contact with the cytoplasmic

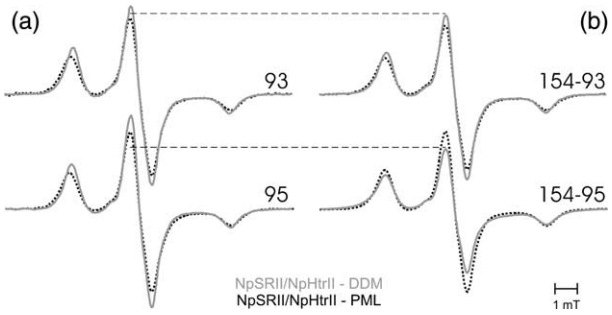

Figure 9. (a) Comparison of low-temperature (160 K) spectra from NpHtrII$_{157}$-L93R1 and NpHtrII$_{157}$-A95R1 in the reconstituted (black dotted line) and solubilized (gray line) NpSRII/NpHtrII$_{157}$ complex. (b) Analogous comparison for two doubly spin-labeled variants NpSRII-S154R1/NpHtrII$_{157}$-L93R1 and NpSRII-S154R1/NpHtrII$_{157}$-A95R1 in the reconstituted (black dotted line) and solubilized (gray line) complex. The spectra are normalized by spin number. The close interaction between the transducer and the receptor is clearly visible in the NpSRII-S154R1/NpHtrII$_{157}$-A95R1 double mutant in the solubilized 1:1 complex by the relevant decrease in intensity of the central peak with respect to the NpSRII/NpHtrII-A95R1 spectrum. The broken horizontal lines are drawn to guide the eyes to better visualize the decrease in intensity of the central peak of the spectra.

region of the receptor in the solubilized 1:1 complex than in the PML-reconstituted 2:2 complex.

Taken together, the observed mobility, accessibility, polarity, and distance changes show that the structure of the transducer in the membrane-proximal region in the solubilized state clearly differs from that in the membrane-reconstituted state.

Discussion

The critical role of lipid–protein interactions has been investigated in a number of studies revealing that function,[4–9,53] and/or protein–protein contacts,[30,54] of membrane proteins are perturbed. Bacteriorhodopsin (BR), for example, a membrane protein related closely to NpSRII, loosens its trimeric structure on solubilization in detergents.[53] Additionally, the well-known effect of the blue shift of the absorption maxima of the dark and light-adapted states of BR upon solubilization is evidence for conformational changes occurring at the level of the retinal-binding pocket.[50,55,56] Furthermore, significant conformational changes were detected for detergent-solubilized BR by NMR studies,[53] pointing to an effect on both transmembrane helices and connecting loops, thereby influencing the functional properties of the protein. Another example is the Ca^{2+}-ATPase from sarcoplasmic reticulum, for which it has been shown that different detergents and, especially, different contents of native lipids in sample preparations strongly influence the oligomerization state of the protein, thereby altering its activity.[4]

The present study exemplifies further the influence of detergents on function, topology, and structure of a membrane protein complex, namely the signaling complex of sensory rhodopsin II and its cognate transducer. Considering the close relationship between BR and the sensory rhodopsin II, strong influences on structure and function, like those observed for BR, are to be expected.

Indeed, the main effects revealed in our study are related to the functional properties, to the oligomerization state, and to the interface between membrane and cytoplasm.

Photocycle

Despite the fact that solubilization does not affect the absorption maxima of NpSRII,[18] differences are observed in the photocycle of the receptor in the detergent-solubilized and in the membrane-reconstituted samples, indicating that the dynamic behavior of the protein is affected by the differences in the molecular order and in the lateral surface energy potential between a lipid bilayer and a detergent micelle. The acceleration of the M decay and the overall faster turnover rates observed for the reconstituted moieties reflect the level of optimization of the photoprocess efficiency in the membrane milieu. Moreover, relevant effects on the reaction cycle of NpSRII are observable after binding of the transducer only in the solubilized samples, thus suggesting a closer interaction between the receptor and the cognate transducer in the solubilized than in the reconstituted complex. Apparently, tighter interactions might not always be correlated to the native state optimized for proper function.

Stoichiometry

The lipid bilayer enables the formation of a 2:2 complex between NpSRII and $NpHtrII_{157}$, which is thought, due to the homologies of the transducer with the dimeric chemoreceptors from enteric bacteria, to be the functional phototactic unit and therefore necessary to retain full functionality of the complex. Moreover, the membrane/vesicle environment has been shown to promote further aggregation of the 2:2 complexes into higher-order clusters. The presence of the membrane triggers the dimerization of the transducer even in the absence of the receptor, showing the structural relevance of the membrane bilayer constraints for the correct assembly of transmembrane proteins. On the contrary, in the solubilized state only a 1:1 stoichiometry is observed between the receptor and the truncated transducer, indicating that the transducer–transducer interaction is hindered or not supported by the detergent. Studies on the 1:1 NpSRII/NpHtrII solubilized complex are therefore necessarily not performed on a fully functional system.

Additionally, it is worth recalling that the truncation performed at position 157 in the transducer is not impairing the tight binding to the receptor, the inhibition of the proton transfer,[24] or the ability of the transducer to trigger the formation of the dimeric functional unit, even in the absence of receptor. On the other hand, the missing cytoplasmic domain, responsible for the four helix bundle formation could remarkably increase the extent of the transducer–transducer interaction, further stabilizing the complex.

Interface

Significant structural differences are observed for the cytoplasmic membrane-proximal domain of the transducer molecule, which seems to be bound more tightly to the receptor in the solubilized rather than in the reconstituted state, as already suggested by the observed altered photocycle of the solubilized complex after transducer binding and by the absence of such effects in the reconstituted complex. Figure 10 shows a model of the 1:1 complex in detergents according to the mobility, accessibility and distance relations data presented here for the membrane-proximal region of the transducer. A recent model presented by Spudich *et al*. for the solubilized NpSRII/NptrII complex is proposing such a close proximity between position

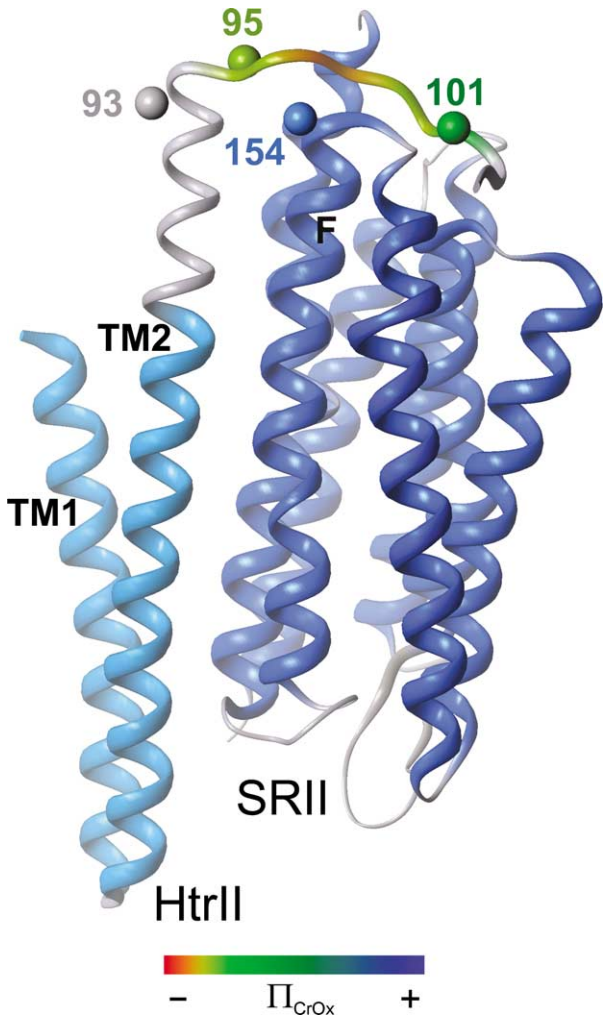

Figure 10. Model proposed for the AS-1 sequence of the HAMP domain of NpHtrII157 in complex with NpSRII in the DDM-solubilized form based on EPR data. Side view of the 1:1 complex with the transducer modeled up to position 101. The NpSRII/NpHtrII transmembrane domain obtained from the X-ray data (PDB 1H2S) is depicted as blue (NpSRII) and cyan (NpHtrII) ribbon representation. The AS-1 sequence up to position 94 is modeled as the α-helical extension of TM2 (gray ribbon); the following 95–101 segment is represented in an extended conformation (according to an EPR model proposed for the 2:2 complex).[46] The segment 95–101 is colored according to the measured CrOx accessibility values. To better visualize the relevant decrease in the water accessibility observed in the solubilized complex with respect to the membrane reconstituted moiety, the CrOx values are scaled according to Figure 7 from Bordignon *et al.*[46] The membrane-adjacent region of the transducer is suggested to interact with the cognate receptor, leading to the observed decrease in side-chain mobility (positions 95–98) and CrOx accessibility (positions 95–101) and to the close contacts observed between residue A95 in the transducer and S154 in the receptor. For clarity, the C^{β} atom of S154 in the receptor is depicted as ball representation; the C^{β} atoms of residues L93, A95 and G101 in the transducer are also depicted and colored according to the Π_{CrOx} values.

S154 in NpSRII and residues S91 to A95 in NpHtrII, which is fully in agreement with our data.[28] Most likely, the structural differences observed in the solubilized with respect to the reconstituted complex arise from both the absence of the second transducer in the 1:1 complex and the differences between the lipid and detergent headgroups, leading to an altered environment for this membrane-associated domain. It is of relevance to note that the membrane-adjacent part of the transducer, thought to be responsible for the signal transduction from the light-activated receptor to the two-component signaling cascade, has been shown to be strongly affected by environmental inputs also in the reconstituted form.[46] This "unstable" functional conformation has been highly optimized during evolution *via* several combined interactions between the transducer and the membrane, the receptor and the cytoplasmic milieu of *N. pharaonis*. Disturbing even one of such interactions may disturb the overall architecture of this functional unit and therefore inhibit the signal transfer.

In conclusion, it has been shown that solubilization of membrane proteins can result in impaired structure and/or function of the molecules under investigation. An important result of the present work concerns the influence of the lipid bilayer on the structural properties of the boundary between membrane and water. This interface region obviously has an important role to confine protein secondary structure.[57] Transmembrane receptors like phototaxis, chemotaxis or tyrosine kinase receptors have to convey the signal from the receptor domain to the cytoplasmic transmitter unit. The linker region connecting the membrane region with the adjacent protein segment might influence both functional correctness and oligomerization. Dimerization of receptor tyrosine kinases has been shown to be the trigger of signal transfer in this class of proteins.[58] This sensitivity of membrane protein complexes towards external conditions like solubilization into detergents has to be taken into account, if the native structure and function has to be evaluated. If possible, membrane-reconstituted samples should be investigated. Recent methodological advances in e.g. EPR spectroscopy and solid state NMR spectroscopy will provide the means to analyze membrane proteins in their natural environment.

Materials and Methods

All measurements were carried out with the NpSRII and the N-terminal fragment of NpHtrII consisting of residues 1–157 (named $NpHtrII_{157}$ for simplicity), both isolated and in complex either being solubilized in DDM or subsequently reconstituted in PML (see Figure 2). For purification purposes, both proteins carry a C-terminal His_7 tag.

Bacterial strains

E. coli XL1 was used as a host for DNA manipulations. Gene expression was carried out in *E. coli* BL21 (DE3).

Cysteine mutants

Starting with the plasmids pET27bmod-NpSRII-His,[59] and pET27bmod-t-HtrII-His (C-terminal truncated transducer (1–157)),[30] cysteine-encoding mutations were introduced using the overlap extension method as described.[60] The final PCR products were ligated into pET27bmod using the NcoI and HindIII restriction sites. Positive clones were verified by DNA sequencing.

Preparation of polar lipids from PM

PMLs were isolated as described.[61] After fast injection of the lipid solution (50 mg/ml of $CHCl_3$/MeOH, 65:35 (v/v) into 25 mM sodium phosphate (pH 8), the resulting suspension was homogenized by sonification and subsequently lyophilized to remove the organic solvents. Rehydration with water to yield a concentration of 2 mg/ml gives a slightly turbid and stable suspension.

Protein expression, spin labeling, and reconstitution in polar lipids

NpSRII-His, $NpHtrII_{157}$-His as well as their respective cysteine mutants were expressed in *E. coli* BL21 (DE3) according to Shimono *et al.*[62] and purified as described.[59] The spin label (1-oxyl-2,2,5,5-tetramethyl-pyrroline-3-methyl)methanethiosulfonate (MTS-SL; TRC, Toronto, Canada) was covalently attached to the cysteine residues of the solubilized NpSRII-His or $HtrII_{157}$-His mutants as described.[45] Excess label was removed by DEAE chromatography. For preparation of the complex, both components were isolated independently and mixed in a 1:1 ratio. The solubilized 1:1 complexes prepared for EPR measurements are in 10 mM Tris–HCl (pH 8.0), 150 mM NaCl, 0.1% (w/v) DDM. For reconstitution into purple membrane lipids (PML), the mixtures were shaken (16 h at 4 °C in the dark) in 10 mM Tris–HCl (pH 8.0), 1 M NaCl containing a 40-fold excess of lipids as well as detergent-absorbing Biobeads (SM2; 10 mg/mg of dodecyl-maltoside (DDM); Boehringer Mannheim). After filtration, the reconstituted proteins were pelleted by centrifugation at 100,000*g* and resuspended in 10 mM Tris–HCl (pH 8.0), 150 mM NaCl.

Laser flash photolysis

The laser flash photolysis setup was essentially identical with that described.[18] The transient absorption changes were recorded at 298 K at 400 nm, 500 nm and 550 nm. Reconstituted complexes were suspended in 10 mM Tris–HCl (pH 7.0), 150 mM NaCl; for solubilized samples the buffer contained additionally 0.1% DDM.

Fluorescence spectroscopy

NpSRII-K157C was labeled with the maleimide functionalized red absorbing dye Atto655 (Atto-TEC GmbH, Siegen, Germany) following standard procedures. Excess of fluorescence dye was removed using a gel-filtration column (Sephadex G-25, Amersham Bioscience). For the fluorescence measurements, the solubilized complex was in detergent buffer (10 mM Tris–HCl (pH 7.2), 150 mM NaCl, 0.1% DDM) at a final concentration of 0.3–0.5 mg/ml. For the reconstitution of the complex into PML, the procedures were applied as described above. Fluorescence emission spectra were recorded using an RF-1501 fluorospectrometer (Shimadzu) with an excitation wavelength of 580 nm. Lifetime measurements were performed with the fluorescence lifetime spectrometer FluoTime200 (PicoQuant, Berlin) using a sub-nanosecond LED source (emission wavelength $\lambda_{max} = 600$ nm). The lifetime of the fluorophore was recorded at an emission wavelength of 680 nm with a repetition rate of 10 MHz. Elastic scattering of the detergent buffer was measured in order to determine the instrument response function (IRF). The measured data were finally fitted using the fluorescence lifetime analysis software FluoFit (PicoQuant, Berlin).

EPR measurements

Room-temperature continuous wave (cw) EPR spectra were recorded using a home-made EPR spectrometer equipped with a Bruker dielectric resonator, with the microwave (MW) power set to 0.4–0.6 mW and B-field modulation amplitude adjusted to 0.15 mT. Samples were loaded into EPR glass capillaries (0.9 mm inner diameter) at final concentrations of 15–20 mg/ml (sample volume 15 μl). Reconstituted samples were prepared as a suspension and the membranes were pelleted by centrifugation in the capillary prior to the measurements. Solubilized samples were prepared in the same buffer containing 0.1% (w/v) DDM.

The accessibility for paramagnetic quenchers, Π, was quantified by the method of continuous wave power saturation.[63] The EPR spectrometer equipped with the Bruker dielectric resonator was used; MW power from 0.1 mW to 30–40 mW was applied to the sample. The protein sample was loaded into a gas-permeable TPX capillary (Spintec). The sample was deoxygenated by a flow of nitrogen gas around the capillary for the reference measurements; for oxygen accessibility measurements, nitrogen was replaced by air; for water accessibility measurements, a chromium oxalate (CrOx) solution was added to the same sample to a final concentration of 50 mM and the nitrogen gas flow was restored. Prior to EPR experiments, the sample was fluxed with the proper gas for 20 min. The errors of the Π values were determined to be in the range of $\pm 10\%$.

EPR spectra for interspin distance determination were recorded at 160 K using a home-made EPR spectrometer equipped with an AEG H103 rectangular cavity. The magnetic field was measured with a B-NM 12 B-field meter (Bruker). A continuous-flow cryostat Oxford ESR 900 allowed stabilization of the sample temperature. The MW power was set to 0.2 mW and the B-field modulation amplitude adjusted to 0.25 mT. Samples were loaded into EPR quartz capillaries (3 mm inner diameter) at final concentrations of 15–20 mg/ml of protein (sample volume 40 μl).

Fitting of simulated dipolar broadened EPR powder spectra to the experimental ones detected at 160 K was performed according to the method described in detail by Steinhoff.[64] The parameters used are $g_{xx} = 2.0086$, $g_{yy} = 2.0066$, $g_{zz} = 2.0026$, $A_{xx} = 0.52$ mT, $A_{yy} = 0.45$ mT, A_{zz} was variable to account for different polarity of the SL environment.[40,41] The spectra were convoluted with a field-independent line-shape function composed of

a superposition of 44% Lorentzian and 56% Gaussian of 0.3 mT and 0.39 mT, respectively.

Acknowledgements

We thank C. Beier for his help with the modeling and visualization of the HAMP domain, and A. Göppner for technical assistance. This work was supported by the Alexander von Humboldt Stiftung (research fellowship for E.B.), the Deutsche Forschungsgemeinschaft (SFB 431/P18, to E.B. and H.-J. S.) and the Max Planck Society (to M.E.).

References

1. Wallin, E. & von Heijne, G. (1998). Genome-wide analysis of integral membrane proteins from eubacterial, archaean, and eukaryotic organisms. *Protein Sci.* **7**, 1029–1038.
2. Sanders, C. R. & Myers, J. K. (2004). Disease-related misassembly of membrane proteins. *Annu. Rev. Biophys. Biomol. Struct.* **33**, 25–51.
3. Geibel, S., Friedrich, T., Ormos, P., Wood, P. G., Nagel, G. & Bamberg, E. (2001). The voltage-dependent proton pumping in bacteriorhodopsin is characterized by optoelectric behavior. *Biophys. J.* **81**, 2059–2068.
4. Lund, S., Orlowski, S., de Foresta, B., Champeil, P., le Maire, M. & Moller, J. V. (1989). Detergent structure and associated lipid as determinants in the stabilization of solubilized Ca^{2+}-ATPase from sarcoplasmic reticulum. *J. Biol. Chem.* **264**, 4907–4915.
5. Banerjee, P., Joo, J. B., Buse, J. T. & Dawson, G. (1995). Differential solubilization of lipids along with membrane proteins by different classes of detergents. *Chem. Phys. Lip.* **77**, 65–78.
6. Haneskog, L., Andersson, L., Brekkan, E., Englund, A. K., Keiichi, K., Liljas, L. *et al*. (1996). Monomeric human red cell glucose transporter (Glut1) in non-ionic detergent solution and a semi-elliptical torus model for detergent binding to membrane proteins. *Biochim. Biophys. Acta*, **1282**, 39–47.
7. Mukhopadhyay, A. K., Bose, S. & Hendler, R. W. (1994). Membrane-mediated control of the bacteriorhodopsin photocycle. *Biochemistry*, **33**, 10889–10895.
8. Joshi, M. K., Dracheva, S., Mukhopadhyay, A. K., Bose, S. & Hendler, R. W. (1998). Importance of specific native lipids in controlling the photocycle of bacteriorhodopsin. *Biochemistry*, **37**, 14463–14470.
9. Dracheva, S., Bose, S. & Hendler, R. W. (1996). Chemical and functional studies on the importance of purple membrane lipids in bacteriorhodopsin photocycle behaviour. *FEBS Letters*, **382**, 209–212.
10. Sanders, C. R., Kuhn Hoffmann, A., Gray, D. N., Keyes, M. H. & Ellis, C. D. (2004). French swimwear for membrane proteins. *ChemBioChem*. **5**, 423–426.
11. Seddon, A. M., Curnow, P. & Booth, P. J. (2004). Membrane proteins, lipids and detergents: not just a soap opera. *Biochim. Biophys. Acta*, **1666**, 105–117.
12. Garavito, R. M. & Ferguson-Miller, S. (2001). Detergents as tools in membrane biochemistry. *J. Biol. Chem.* **276**, 32403–32406.
13. Haupts, U., Tittor, J. & Oesterhelt, D. (1999). Closing in on bacteriorhodopsin: progress in understanding the molecule. *Annu. Rev. Biophys. Biomol. Struct.* **28**, 367–399.
14. Schäfer, G., Engelhard, M. & Müller, V. (1999). Bioenergetics of the Archaea. *Microbiol. Mol. Biol. Rev.* **63**, 570–620.
15. Spudich, J. L., Yang, C.-S., Jung, K.-H. & Spudich, E. N. (2000). Retinylidene proteins: structures and functions from Archaea to humans. *Annu. Rev. Cell Dev. Biol.* **16**, 365–392.
16. Spudich, J. L. & Luecke, H. (2002). Sensory rhodopsin II: functional insights from structure. *Curr. Opin. Struct. Biol.* **12**, 540–546.
17. Klare, J. P., Gordeliy, V. I., Labahn, J., Buldt, G., Steinhoff, H. J. & Engelhard, M. (2004). The archaeal sensory rhodopsin II/transducer complex: a model for transmembrane signal transfer. *FEBS Letters*, **564**, 219–224.
18. Chizhov, I., Schmies, G., Seidel, R. P., Sydor, J. R., Lüttenberg, B. & Engelhard, M. (1998). The photophobic receptor from *Natronobacterium pharaonis*: temperature and pH dependencies of the photocycle of sensory rhodopsin II. *Biophys. J.* **75**, 999–1009.
19. Wegener, A. A., Chizhov, I., Engelhard, M. & Steinhoff, H.-J. (2000). Time-resolved detection of transient movement of helix F in spin-labelled pharaonis sensory rhodopsin II. *J. Mol. Biol.* **301**, 881–891.
20. Klare, J. P., Bordignon, E., Engelhard, M. & Steinhoff, H.-J. (2004). Sensory rhodopsin II and bacteriorhodopsin: light activated helix F movement. *Photochem. Photobiol. Sci.* **3**, 543–547.
21. Hoff, W. D., Jung, K.-H. & Spudich, J. L. (1997). Molecular mechanism of photosignalling by archaeal sensory rhodopsins. *Annu. Rev. Biophys. Biomol. Struct.* **26**, 223–258.
22. Sudo, Y., Iwamoto, M., Shimono, K. & Kamo, N. (2001). *Pharaonis* phoborhodopsin binds to its cognate truncated transducer even in the presence of a detergent with a 1:1 stoichiometry. *Photochem. Photobiol*. **74**, 489–494.
23. Sudo, Y., Okuda, H., Yamabi, M., Fukuzaki, Y., Mishima, M., Kamo, N. & Kojima, C. (2005). Linker region of a halobacterial transducer protein interacts directly with its sensor retinal protein. *Biochemistry*, **44**, 6144–6152.
24. Hippler-Mreyen, S., Klare, J. P., Wegener, A. A., Seidel, R., Herrmann, C., Schmies, G. *et al*. (2003). Probing the sensory rhodopsin II binding domain of its cognate transducer by calorimetry and electrophysiology. *J. Mol. Biol.* **330**, 1203–1213.
25. Sudo, Y., Iwamoto, M., Shimono, K. & Kamo, N. (2002). Association between a photo-intermediate of a M-lacking mutant D75N of pharaonis phoborhodopsin and its cognate transducer. *J. Photochem. Photobiol. B*, **67**, 171–176.
26. Sudo, Y., Iwamoto, M., Shimono, K. & Kamo, N. (2002). Tyr-199 and charged residues of pharaonis phoborhodopsin are important for the interaction with its transducer. *Biophys. J.* **83**, 427–432.
27. Furutani, Y., Kamada, K., Sudo, Y., Shimono, K., Kamo, N. & Kandori, H. (2005). Structural changes of the complex between pharaonis phoborhodopsin and its cognate transducer upon formation of the M photointermediate. *Biochemistry*, **44**, 2909–2915.
28. Yang, C. S., Sineshchekov, O., Spudich, E. N. & Spudich, J. L. (2004). The cytoplasmic membrane-proximal domain of the HtrII transducer interacts

with the E-F loop of photoactivated natronomonas pharaonis sensory rhodopsin II. *J. Biol. Chem.* **279**, 42970–42976.
29. Gordeliy, V. I., Labahn, J., Moukhametzianov, R., Efremov, R., Granzin, J., Schlesinger, R. *et al*. (2002). Molecular basis of transmembrane signalling by sensory rhodopsin II-transducer complex. *Nature*, **419**, 484–487.
30. Wegener, A. A., Klare, J. P., Engelhard, M. & Steinhoff, H.-J. (2001). Structural insights into the early steps of receptor-transducer signal transfer in archaeal phototaxis. *EMBO J.* **20**, 5312–5319.
31. Sudo, Y., Yamabi, M., Iwamoto, M., Shimono, K. & Kamo, N. (2003). Interaction of Natronobacterium pharaonis phoborhodopsin (sensory rhodopsin II) with its cognate transducer probed by increase in the thermal stability. *Photochem. Photobiol.* **78**, 511–516.
32. Sasaki, J. & Spudich, J. L. (1998). The transducer protein HtrII modulates the lifetimes of sensory rhodopsin II photointermediates. *Biophys. J.* **75**, 2435–2440.
33. Sudo, Y., Iwamoto, M., Shimono, K., Sumi, M. & Kamo, N. (2001). Photo-induced proton transport of *pharaonis* phoborhodopsin (sensory rhodopsin II) Is Ceased by association with the transducer. *Biophys. J.* **80**, 916–922.
34. Buschmann, V., Weston, K. D. & Sauer, M. (2003). Spectroscopic study and evaluation of red-absorbing fluorescent dyes. *Bioconjug. Chem.* **14**, 195–204.
35. Marme, N., Knemeyer, J.-P., Sauer, M. & Wolfrum, J. (2003). Inter- and intramolecular fluorescence quenching of organic dyes by tryptophan. *Bioconjug. Chem.* **14**, 1133–1139.
36. Maddock, J. R. & Shapiro, L. (1993). Polar location of the chemoreceptor complex in the *Escherichia coli* cell. *Science*, **259**, 1717–1723.
37. Shimizu, T. S., Le Novere, N., Levin, M. D., Beavil, A. J., Sutton, B. J. & Bray, D. (2000). Molecular model of a lattice of signalling proteins involved in bacterial chemotaxis. *Nature Cell Biol.* **2**, 792–796.
38. Henderson, R. & Unwin, P. N. T. (1975). Three-dimensional model of purple membrane obtained by electron microscopy. *Nature*, **257**, 28–32.
39. Kim, S. H., Wang, W. & Kim, K. K. (2002). Dynamic and clustering model of bacterial chemotaxis receptors: structural basis for signaling and high sensitivity. *Proc. Natl Acad. Sci. USA*, **99**, 11611–11615.
40. Hubbell, W. L., Mchourab, H. S., Altenbach, C. & Lietzow, M. A. (1996). Watching Proteins move using site-directed spin labeling. *Structure*, **4**, 779–783.
41. Hubbell, W. L., Gross, A., Langen, R. & Lietzow, M. A. (1998). Recent advances in site-directed spin labeling of proteins. *Curr. Opin. Struct. Biol.* **8**, 649–656.
42. Berliner, L. J. (1998). *Spin Labeling: The Next Millennium*, Academic Press, New York.
43. Steinhoff, H.-J. (2002). Methods for study of protein dynamics and protein–protein interaction in protein-nubiquitination by electron paramagnetic resonance spectroscopy. *Front. Biosci.* **7**, c97–c110.
44. Altenbach, C., Marti, T., Khorana, H. G. & Hubbell, W. L. (1990). Transmembrane protein structure: spin labeling of bacteriorhodopsin mutants. *Science*, **248**, 1088–1092.
45. Pfeiffer, M., Rink, T., Gerwert, K., Oesterhelt, D. & Steinhoff, H.-J. (1999). Site-directed spin-labeling reveals the orientation of the amino acid side-chains in the E-F loop of bacteriorhodopsin. *J. Mol. Biol.* **287**, 163–171.
46. Bordignon, E., Klare, J. P., Doebber, M., Wegener, A. A., Martell, S., Engelhard, M. & Steinhoff, H.-J. (2005). Structural analysis of a HAMP domain: the linker region of the phototransducer in complex with sensory rhodopsin II. *J. Biol. Chem.* **280**, 38767–38775.
47. Mchaourab, H. S., Lietzow, M. A., Hideg, K. & Hubbell, W. L. (1996). Motion of spin-labeled side chains in T4 Lysozyme. Correlation with protein structure and dynamics. *Biochemistry*, **35**, 7692–7704.
48. Hubbell, W. L., Cafiso, D. S. & Altenbach, C. (2000). Identifying conformational changes with site-directed spin labeling. *Nature Struct. Biol.* **7**, 735–739.
49. Medina, R., Perdomo, D. & Bubis, J. (2004). The hydrodynamic properties of dark- and light-activted states of n-dodecyl β-D-maltoside-solubilized bovine rhodopsin support the dimeric structure of both conformations. *J. Biol. Chem.* **279**, 39565–39573.
50. Meyer, O., Ollivon, M. & Paternostre, M. T. (1992). Solubilization steps of dark-adapted purple membrane by Triton X-100: a spectroscopic study. *FEBS Letters*, **305**, 249–253.
51. Steinhoff, H.-J., Savitsky, A., Wegener, C., Pfeiffer, M., Plato, M. & Möbius, K. (2000). High-field EPR studies of the structure and conformational changes of site-directed spin labeled bacteriorhodopsin. *Biochim. Biophys. Acta*, **1457**, 253–262.
52. Plato, M., Steinhoff, H.-J., Wegener, C., Törring, J. T., Savitsky, A. & Möbius, K. (2002). Molecular orbital study of polarity and hydrogen bonding effects on the g and hyperfine tensors of site directed NO spin labelled bacteriorhodopsin. *Mol. Phys.* **100**, 3711–3721.
53. Tanio, M., Tuzi, S., Yamaguchi, S., Konishi, H., Naito, A., Needleman, R. *et al*. (1998). Evidence of local conformational fluctuations and changes in bacteriorhodopsin, dependent on lipds, detergents and trimeric structure, as studied by ^{13}C NMR. *Biochim. Biophys. Acta*, **1375**, 84–92.
54. Stanley, A. M. & Fleming, K. G. (2005). The transmembrane domains of ErbB receptors do not dimerize strongly in micelles. *J. Mol. Biol.* **347**, 759–772.
55. Gonzalez-Manas, J. M., Montoya, G., Rodriguez-Fernandez, C., Gurtubay, J. I. G. & Goni, F. M. (1990). The interaction of Triton X-100 with purple membrane: effect of light-dark adaptation. *Biochim. Biophys. Acta*, **1019**, 167–169.
56. Kovacs, I., Hollos-Nagy, K. & Varo, G. (1995). Dark adaptation and spectral changes in Triton X-100-treated bacteriorhodopsin. *J. Photochem. Photobiol. B*, **27**, 21–25.
57. Liang, J., Adamian, L. & Jackups, J. (2005). The membrane-water interface region of membrane proteins: structural bias and the anti-snorkeling effect. *Trends Biochem. Sci.* **30**, 355–357.
58. Hubbard, S. R. & Till, J. H. (2000). Protein tyrosine kinase structure and function. *Annu. Rev. Biochem.* **69**, 373–398.
59. Hohenfeld, I. P., Wegener, A. A. & Engelhard, M. (1999). Purification of Histidine tagged bacteriorhodopsin *pharaonis* halorhodopsin and *pharaonis* sensory rhodopsin II functionally expressed in *Escherichia coli*. *FEBS Letters*, **442**, 198–202.
60. Ho, S. N., Hunt, H. D., Horton, R. M., Pullen, J. K. & Pease, L. R. (1989). Site-directed mutagenesis by overlap extension using the polymerase chain reaction. *Gene*, **77**, 51–59.

61. Kates, M., Kushawa, S. C. & Sprott, G. D. (1982). Lipids of purple membrane from extreme halophiles and of methanogenic bacteria. *Methods Enzymol.* **88**, 98–111.
62. Shimono, K., Iwamoto, M., Sumi, M. & Kamo, N. (1997). Functional expression of *pharaonis* phoborhodopsin in *Escherichia coli*. *FEBS Letters*, **420**, 54–56.
63. Altenbach, C., Greenhalgh, D. A., Khorana, H. G. & Hubbell, W. L. (1994). A collision gradient method to determine the immersion depth of nitroxides in lipid bilayers: application to spin-labeled mutants of bacteriorhodopsin. *Proc. Natl Acad. Sci. USA*, **91**, 1667–1671.
64. Steinhoff, H.-J., Radzwill, N., Thevis, W., Lenz, V., Brandenburg, D. & Antson, A. (1997). Determination of interspin distances between spin labels attached to insulin: comparison of electron paramagnetic resonance data with the X-ray structure. *Biophys. J.* **73**, 3287–3298.

Edited by I. B. Holland

(Received 29 August 2005; received in revised form 2 December 2005; accepted 4 December 2005)
Available online 20 December 2005